ACS APPLIED MATERIALS & INTERFACES

www.acsami.org Research Article

Putting Ink into Polyion Micelles: Full-Color Anticounterfeiting with Water/Organic Solvent Dual Resistance

Tongyue Wu, Mengqi Xie, Jianbin Huang,* and Yun Yan*

Cite This: *ACS Appl. Mater. Interfaces* 2020, 12, 39578−39585 Read Online

ACCESS | Metrics & More | Article Recommendations | Supporting Information

ABSTRACT: Anticounterfeiting paintings are usually with limited colors and easy blurring and need to be dispersed in an environmentally unfriendly organic solvent. We report a set of water-based polyion micellar inks to solve all these problems. Upon complexation of reversible coordination polymers formed with rare earth metal ions Eu^{3+} and Tb^{3+} and the aggregation-induced emission ligand tetraphenylethylene-L_2EO_4 with oppositely charged block polyelectrolyte $P2MVP_{29}$-*b*-PEO_{205}, we are able to generate polyion micelles displaying three elementary emission colors of red (R) ($\Phi_{Eu^{3+}}$ = 24%), green (G) ($\Phi_{Tb^{3+}}$ = 7%), and blue (B) (Φ_{TPE} = 9%). Full-spectrum emission and white light emission (0.34, 0.34) become possible by simply mixing the R, G, and B micelles at the desired fraction. Strikingly, the micellar inks remain stable even after soaking in water or organic solvents (ethyl acetate, ethanol, etc.) for 24 h. We envision that polyion micelles would open a new paradigm in the field of anticounterfeiting.

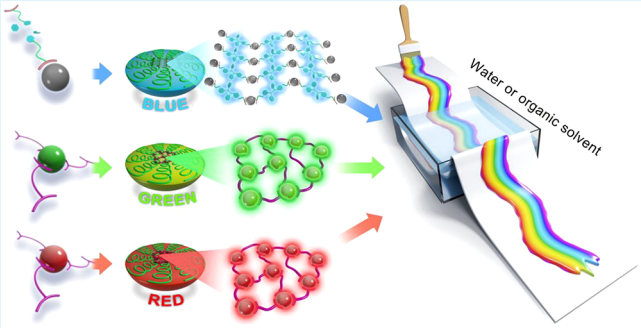

KEYWORDS: *anticounterfeiting, micelles, coordination, rare earth metal ions, aggregation-induced emission*

INTRODUCTION

Data security is of paramount importance in fields ranging from economy, military, and politics.[1−6] Counterfeiting has serious threats to the safety of these fields.[7] Over the past centuries, a wide variety of anticounterfeiting technologies have been developed,[8−11] such as watermarks,[12,13] intaglio printing,[14] luminescent ink,[15−23] anticounterfeiting paper,[24−26] and electronic tracking using radio frequency identification.[27] Among them, luminescent ink[15,16,18−23,28] is very attractive owing to its convenience in application.[10] Anticounterfeiting luminescent inks are usually organic solutions of organic dyes,[29−34] quantum dots,[24,35−37] inorganic nanoparticles,[38−41] and perovskite nanocrystals.[42−44] Patterns made with these inks are invisible under daylight, but can be detected by a specific instrument.[45]

Most of the current anticounterfeiting inks suffer from a number of problems, such as (i) limited color choice[24,36] and broad emission peak which may cause poor specificity and security,[31] (ii) poor resolution due to the weak fluorescence aroused from the notorious aggregation caused quenching of conventional dyes,[30] (iii) low biocompatibility[46,47] due to the use of the organic solvent, and (iv) requirement of extra protection layers[25] to avoid blurring of paintings when exposed to the solvent.[22] All these disadvantages hinder their practical applications.

Herein, we report that aqueous anticounterfeiting ink built with polyion complex micelles[48,49] (PICMs) could overcome all the aforementioned problems. We show that upon incorporating red (R) and green (G) emission from rare earth metal ions (Eu^{3+} and Tb^{3+}) and blue (B) emission from aggregation-induced emission (AIE) fluorophore [tetraphenylethylene (TPE)] into different reversible coordination supramolecular polymers,[50,51] PICMs can be constructed in water when these supramolecular polymers electrostatically complex with an oppositely charged block copolymer (Scheme 1). The RGB elements are sealed in the micellar core, and they are independent of each other. As a result, full-color aqueous micellar ink could be obtained by simply mixing the RGB elements at the desired ratio. It is striking that the formation of PICMs significantly enhances the solvent resistance of the anticounterfeiting paintings. When paintings made with unmicellized RGB inks were immediately blurred upon coming into contact with water, the PICM paintings remain stable even after soaking in water for 24 h (Scheme 1). Moreover, these water-based micellar paintings also display resistance to various organic solvents. Finally, we show that these PICM inks, which consist of small micelles with an average hydrodynamic radius of 8−14 nm, can be applied in a commercial inkjet printer for anticounterfeiting application.

Received: June 7, 2020
Accepted: August 4, 2020
Published: August 4, 2020

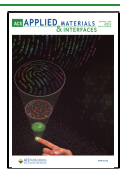

https://dx.doi.org/10.1021/acsami.0c10355
ACS Appl. Mater. Interfaces 2020, 12, 39578−39585

Scheme 1. Illustration of the PICM Ink Composed of RGB Three-Color Elements Displaying Full-Spectrum Anticounterfeiting Ability with Water/Organic Solvent Dual Resistance

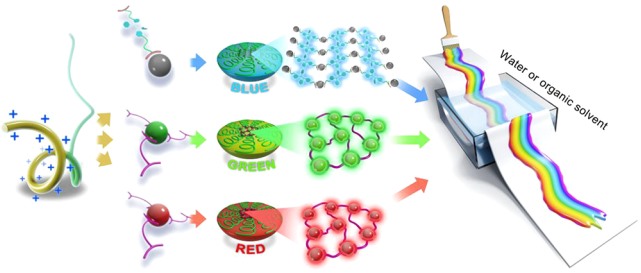

Owing to the different widths of the excitation window for rare earth metal ions and the TPE group, the obtained anticounterfeiting paintings display excitation-dependent colors. All these advantages suggest that PICMs could be a potent system leading to advanced anticounterfeiting inks.

■ RESULTS AND DISCUSSION

To generate individual R, G, and B emission,[52−54] two groups of negatively charged coordination polymers are used in this study. One is formed with luminescent rare earth metal ions (Eu^{3+} and Tb^{3+})[52,55−57] and nonemissive ligand L_2EO_4 (Scheme 2a),[52,55−57] and the other is formed with the nonemissive transition metal ion Zn^{2+} and bisligand containing the AIE moiety TPE (Scheme 2b).[58] Upon addition of the positively charged block copolymer poly(*N*-methyl-2-vinylpyridinium iodide)-*b*-poly(ethylene oxide)[52,55−60] ($P2MVP_{29}$-*b*-PEO_{205}, as illustrated in Scheme 2c) to the aqueous solution of different reversible coordination supramolecular polymers, luminescent core−shell micelles displaying red (R), green (G), and blue (B) emission can be generated (Scheme 1), where the R, G, and B elements are from the Eu-, Tb-, and TPE-coordination supramolecular polymers in the micellar core, respectively.

The aqueous solution of the single component of $P2MVP_{29}$-PEO_{205} and the coordination polymers Eu/L_2EO_4, Tb/L_2EO_4, and Zn/TPE-L_2EO_4 do not form micelles (Figures S1−S3). However, dynamic light scattering (DLS, Figure 1a) and transmission electron microscopy (TEM, Figures 1b, and S4) confirm the formation of micelles in the mixed systems at the charge-balancing ratio of [+]/[−] = 1:1. The particle radius obtained with DLS is 8−12 nm, which is the overall size of the core and shell for PICMs.[58] The size of the micellar core read from the TEM observation is about 5−8 nm.[59,60] This is because the shell of the PICMs is water-swollen which is hardly discernible by TEM.[61] Only the core with metal ions displays sufficient contrast under TEM observation (Figure 1c).[59,62]

The inset in Figure 1a is the photograph of the three micellar suspensions under 254 nm UV light, which are red, green, and blue (cyan). Spectral measurements (Figure 1d) reveal that the Eu micelle shows characteristic europium luminescence at 595, 614, and 694 nm under 254 nm excitation, corresponding to $^5D_0$−$^7F_1$, $^5D_0$−$^7F_2$, and $^5D_0$−$^7F_4$ transitions of europium, respectively.[63] Analogously, the Tb micelle shows the characteristic f−f transition peak of terbium at 494, 544, 587, and 622 nm, corresponding to $^5D_4$−$^7F_6$, $^5D_4$−$^7F_5$, $^5D_4$−$^7F_4$, and $^5D_4$−$^7F_3$, respectively.[63] These spectrum features indicate that the rare earth metal ion Eu^{3+} and Tb^{3+} emissions have been sensitized by the coordinating

Scheme 2. Illustration of the Molecular Structure of (a) L_2EO_4 and Eu/Tb Coordination Polymers. Re^{3+} Represents Eu^{3+} or Tb^{3+}. (b) Structure of the TPE-L_2EO_4 Ligand and TPE-Zn Coordination Polymer; (c) structure of the Block Polyelectrolyte $P2MVP_{29}$-PEO_{205}

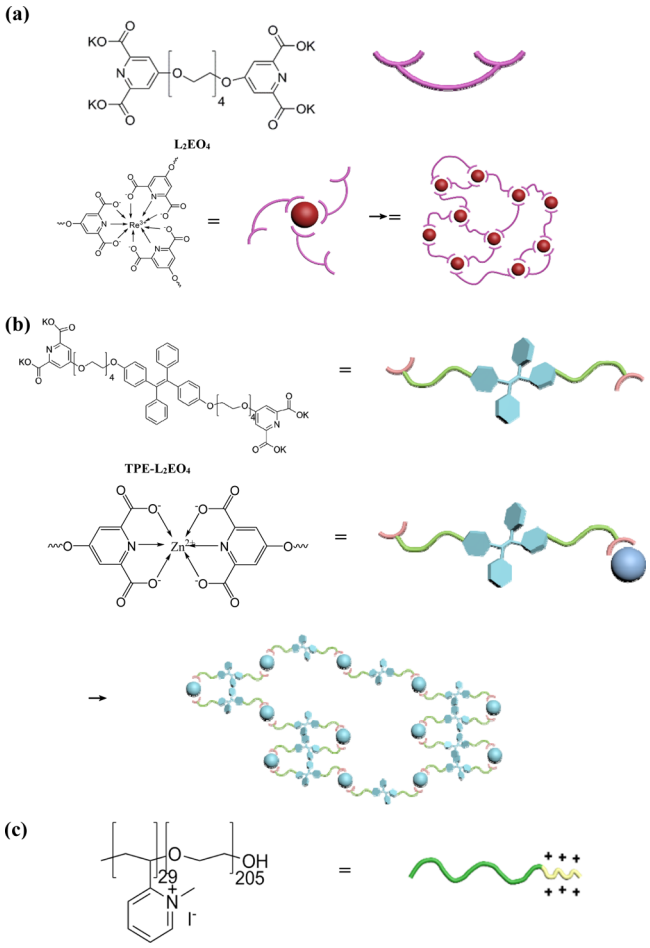

antenna of pyridine dicarboxylate in water. Different from these narrow rare earth metal emissions, the TPE micelle shows a broad emission band centering at 489 nm, featuring the emission of the TPE group.[58,64−66] The quantum yields for the three micelles are $\Phi_{Eu^{3+}}$ = 24%,$\Phi_{Tb^{3+}}$ = 7%, and Φ_{TPE} = 9%, and their CIE coordinates can be obtained as (0.66, 0.33), (0.35, 0.57), and (0.22, 0.35), respectively (Figure 1e). These results suggest that the formation of micelles have drastically enhanced the luminescence ability of the two rare earth metal ions and the TPE group because none of them display applicable emissions before micellization (Figures S1−S3).

Because R, G, and B are the three primary colors of white light, we expect to obtain the full spectrum of emission from these inks upon mixing them at various fractions. For instance, as the molar fraction of Eu micelles and TPE micelles varies from 1:0 to 0:1, the emission color of the ink gradually changes from red to blue (Figure 2a). Spectral measurements reveal that the intensity for the red emission is proportional to the fraction of the Eu micelle, while the blue component is proportional to the fraction of the TPE micelle (Figure S5). This gradual change can also be seen in the CIE plot, where the color coordinates shift from the red corner linearly to the blue region, confirming the quantitative variation of the red and green emission components (lower inset in Figure 2a).

https://dx.doi.org/10.1021/acsami.0c10355
ACS Appl. Mater. Interfaces 2020, 12, 39578−39585

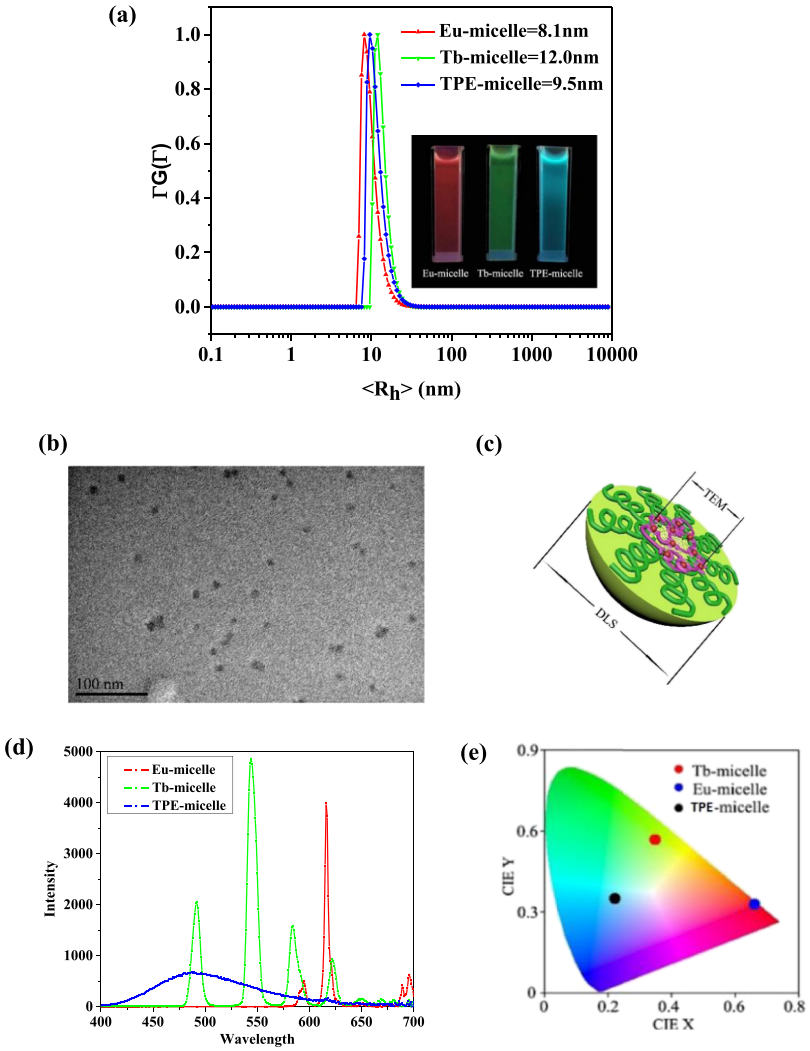

Figure 1. Structure and spectral information of PICMs. (a) DLS result for the Eu micelle, Tb micelle, and TPE micelle, respectively. The inset is the fluorescent photographs of the micellar inks. (b) TEM image of the Tb micelle (R_{core} = 6.9 nm). (c) Schematic illustration of the sizes obtained from DLS and TEM measurements. (d) Emission spectra of the three micelles under 254 un UV light (Eu micelle: 50 μmol/L and Tb micelle and Zn micelle: 200 μmol/L). (e) CIE coordinate diagram of the three micelles.

DLS measurements (Figure 2b) suggest the presence of only one group of particles of R_h = 14 nm in the mixed micellar system. This size is larger than the individual Eu, Tb, and TPE micelles, indicating that these micelles have probably rearranged in water so that the core materials are mixed at the molecular level. Although this information cannot be differentiated in the normal TEM image (Figure S6), we found that the emission color of the micelles is always the same, no matter by mixing two different micelles or by mixing the metal ions or coordination polymers before micelle formation (Figure S7). This means that the RGB emissions are independent at the molecular level so that they would not interfere with each other, which lays very good foundation for their application as a set of inks. As expected, the emission color evolutes from red to green as the molar ratio of Eu and Tb micelles is varied (Figure S8). These micelles are all stable in a broad pH window of 3−11 (Figure S9) and can survive in ionic strength 10 times of their own concentration (Figure S10).

It is worth noting that a white emission with the CIE coordinate being (0.34, 0.34) can be obtained as the molar ratio of the TPE micelle: Eu micelle reaches 75:25 (Figure 2c), which is very close to the CIE coordinates of the standard white emission (0.33, 0.33).

Paintings made with these micellar inks are invisible under natural light (Figure S11a). However, bright images are observed under 254 nm UV irradiation. Figure 3a,b is the drawings made with individual Eu, Tb, and TPE micelles on filter paper. The sunflower in Figure 3c is, however, pained with the mixed Eu and Tb micelles. No detectable luminescence and color changes occur for these paintings within 12 months, indicating that the luminescence property was preserved in the solid state. Actually, the spectral measurements reveal that the luminescence of the ink remains nearly unchanged after the sample was kept under daylight for 27 months, and the change in luminescence is acceptable under 4−6 h of constant 254 nm 12 W UV light irradiation (Figure S12).

It is striking that the paintings made with these micellar inks are all water-resistant (Figure S13) even after being soaked in water for 24 h. In contrast, the patterns made with unmicellized coordination polymers (Figure S11b,c) would disappear within 1 min after soaking. Figure 3d shows a pattern of the Chinese character "王" with the top "—" written in the

https://dx.doi.org/10.1021/acsami.0c10355
ACS Appl. Mater. Interfaces 2020, 12, 39578−39585

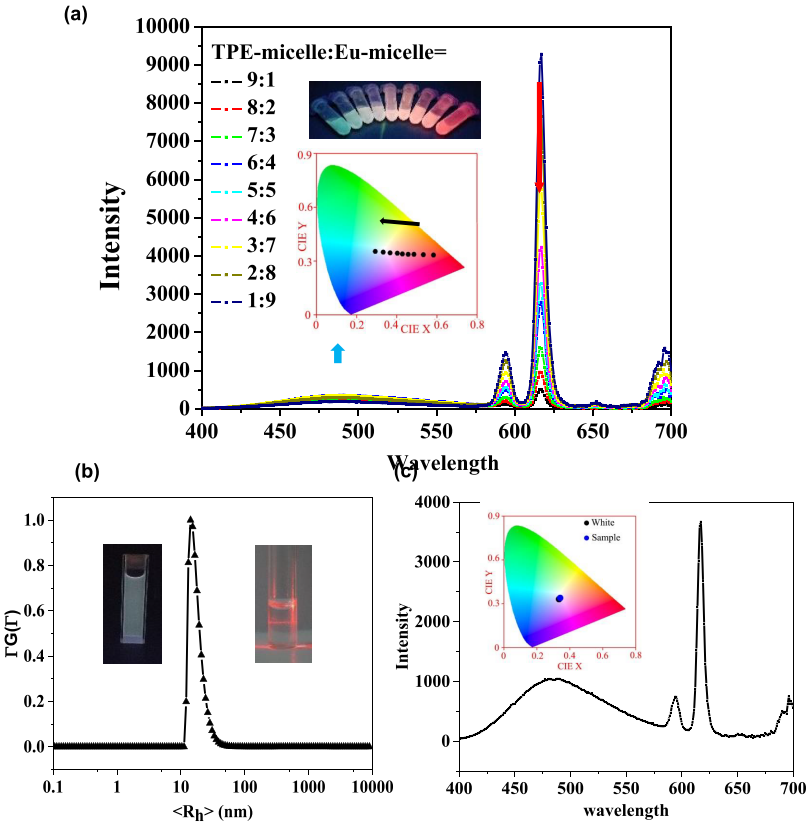

Figure 2. Demonstration of a full spectrum emission by simply mixing the TPE- and Eu-micellar inks at different molar ratios. Fluorescence spectrum and CIE coordinate (a) variation of the fluorescence spectrum with the molar fraction of TPE and Eu micelles. Upper inset: photographs of the mixed TPE micelle and Eu micelle at different molar ratios. Lower inset: CIE plot of the Eu/TPE mixed micelles. (b,c) DLS result and fluorescent spectrum of the white-emissive system composed of TPE micelle: Eu micelle = 75:25. The insets in (b) are the fluorescent photographs of white-emissive micellar ink under 254 nm UV irradiation (left) and the Tyndall effect of the system (right). The inset in (c) is the CIE coordinate of the white-emissive micellar ink (0.34, 0.34) and of standard white light (0.33, 0.33).

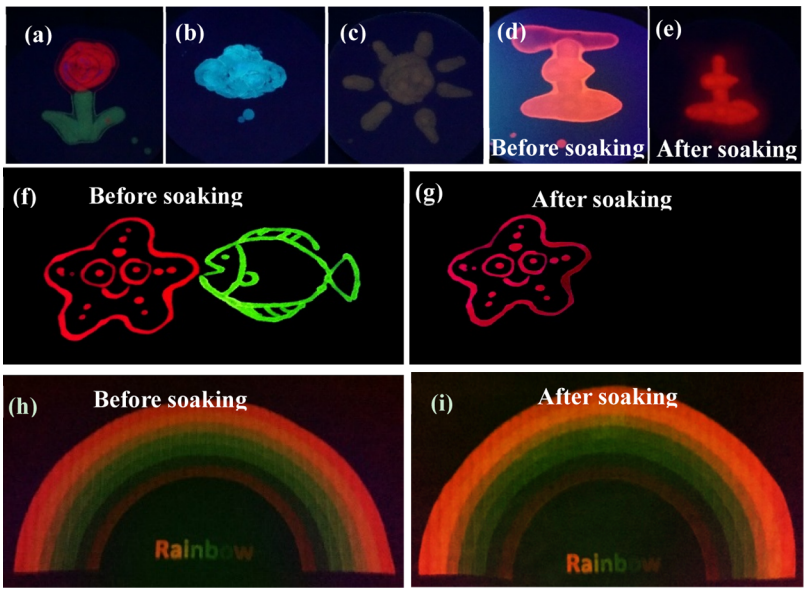

Figure 3. Luminescent images painted or printed with the micellar ink under different conditions. (a) Red flower and a green grass written with Eu and Tb micelles, respectively, on filter paper; (b) blue cloud painted with the TPE micelle on filter paper; (c) yellow sun painted with the mixed ink of Eu and Tb micelles on filter paper. (d,e) Patterns painted partially with the Eu-L_2EO_4 supramolecular ink and partially with the Eu-micellar ink before and after soaking in water on a filter paper. The Eu-L_2EO_4 ink painting vanishes after being soaked in water for 1 min, whereas that painted with Eu-micellar ink remains even after 24 h. (f,g) Paintings made with the Eu micelle and Tb-L_2EO_4 coordination polymers under 254 nm UV irradiation before and after soaking in water on filter paper. (h,i) Paintings made with an inkjet printer under 254 nm using the Eu and Tb micelles as the R and G red ink boxes on a commercial A4 paper. All the images were taken under 254 nm UV light.

https://dx.doi.org/10.1021/acsami.0c10355
ACS Appl. Mater. Interfaces 2020, 12, 39578−39585

L_2EO_4 + Eu^{3+} ink, while the "⊥" below is written in Eu-micellar ink. After soaking in water for 1 min, the top "—" is washed away and the below "⊥" is left (Figure 3e). Figure 3f,g shows a similar water-resistant test made with the red Eu-micellar ink and the green L_2EO_4 + Tb^{3+} ink. The bright green fish vanishes completely after soaking the pattern in water for 1 min, but the red starfish is still there even after 24 h. Obviously, the formation of micelles has greatly increased the affinity of the micelles to the paper tissue. This is because the poly(ethylene oxide) (PEO) chains have great affinity to paper tissue,[25,67,68] which retains the ink in the paper. It should be noted that the paintings made with the aqueous micellar ink also resist various organic solvents, such as ethanol, methanol, benzene, alkanes, and ethyl acetate, which makes it possible to make robust anticounterfeiting images (Figure S14).

Because the Eu, Tb, and TPE micelles have a similar structure and their emissions do not interfere with each other, this allows us to fill these inks into a commercial ink box to demonstrate their ability in practical printings. Figures 3h,i and S15 demonstrate the printed patterns of a rainbow and letters on a commercial A4 paper. It is noticed that the resolution of the painting is sufficiently high so that the details of the painting are clearly identified. Strikingly, after being soaked in water for 24 h, both the printings remain clear with negligible fading and blurring. Finally, this set of anticounterfeiting ink displays excitation wavelength-dependent emission. Because the AIE moiety TPE can be exited in a broad range of wavelength (Figure S16a), the blue emission from the TPE micelle remains as the excitation wavelength shifts from 254 to 365 nm, whereas that from the Eu and Tb micelles vanishes (Figure S16b). Therefore, this set of full-spectrum leaking-resistant micellar inks also displays dual-wavelength detection, rendering extra safety in anticounterfeiting.

■ CONCLUSIONS

In summary, we report a water-based polyion micellar ink that displays full-spectral colors by combination of AIE and luminescence of rare earth metals. With the reversible coordination polymers formed out of rare earth metals and AIE ligands, micelles displaying individual colors of red, green, and blue are fabricated, which immediately generates full-spectrum emission upon simply mixing the R, G, and B micelles at the desired fraction. Compared with unmicellized coordination polymers, the micelles have strong affinity to paper tissue so that the paintings made with the micellar ink remains stable even after soaking in water or organic solvents. We expect that the present luminescent micellar ink opens a new paradigm for the development of anticounterfeiting technology, which may promote the data security in fields ranging from politics, economy, military, and even national defenses.

■ EXPERIMENTAL SECTION

Synthesis of the Bifunctional Ligand TPE-$(EO)_4$-L_2 and L_2EO_4. TPE-$(EO)_4$-L_2 (L: dicarboxypyridine group) and 1,11-bis(2,6-dicarboxypyridin-4-yloxy)-3,6,9-trioxaundecane (L_2EO_4) used in this work were synthesized according to previously reported procedures.[53,69]

Other Materials. Diblock polyelectrolyte $PMVP_{29}$-*b*-PEO_{205} (M_w = 16k, PDI = 1.3, about 90% quaternized) used in this work was prepared by following a procedure described elsewhere.[70] Diblock polymer poly(2-vinylpyridine)-*b*-poly (ethylene oxide) ($P2VP_{29}$-*b*-PEO_{205}, M_w = 12k, PDI = 1.3) was obtained from Polymer Science. $Eu(NO_3)_3{\cdot}6H_2O$ (99.99%) and $Tb(NO_3)_3{\cdot}6H_2O$ (99.99%) were obtained from Sigma and used without further purification. Distilled water was purified through a Milli-Q Advantage A10 ultrapure water system. The other chemicals were obtained from Beijing Chemical Reagents Co., and all were of A.R. grade.

Sample Preparation. Stock solutions of $PMVP_{29}$-*b*-PEO_{205}, L_2EO_4, TPE-$(EO)_4$-L_2, $Tb(NO_3)_3$, $Zn(NO_3)_2$, and $Eu(NO_3)_3$ were prepared at appropriate concentrations. In order to prepare the L_2EO_4 + Eu^{3+} micelle, 1 mM L_2EO_4 solution and 10 mM $Eu(NO_3)_3$ solution were mixed at desired molar ratios. The coordination complexes were added in stoichiometric amounts to a $PMVP_{29}$-*b*-PEO_{205} aqueous solution (positive charge concentration 10 mM) to reach charge neutral mixing. The L_2EO_4 + Tb^{3+} micelle is prepared in the same method. The TPE + Zn^{2+} micelle is prepared by adding TPE-L_2EO_4, $PMVP_{29}$-PEO_{205}, and $Zn(NO_3)_2$, orderly, with TPE-L_2EO_4 and $Zn(NO_3)_2$ at the same concentration, and $PMVP_{29}$-PEO_{205} is added till electrostatic equilibrium. Metal-coordinated supramolecules, L_2EO_4/Eu^{3+} = 3:2 and L_2EO_4/Tb^{3+} = 3:2, are prepared by mixing L_2EO_4 with $Eu(NO_3)_3$ or $Tb(NO_3)_3$ to the proper ratio. HCl and NaOH were used to control the pH.

Printing with an Inkjet Printer. An aqueous mixture of 2.500 mM $Zn(NO_3)_2$, 2.500 mM TPE-$(EO)_4$-L_2, and 0.192 mM $PMVP_{29}$-PEO_{205} was prepared as the blue emission ink. Similarly, an aqueous mixture of 0.667 mM $Eu(NO_3)_3$, 1.000 mM L_2EO_4, and 0.077 mM $PMVP_{29}$-PEO_{205} was prepared as the red emission ink, and an aqueous mixture of 1.667 mM $Tb(NO_3)_3$, 2.500 mM L_2EO_4, and 0.192 mM $PMVP_{29}$-PEO_{205} was prepared as the green emission ink. The fluorescence intensities of these solutions were nearly identical with an excitation wavelength of 254 nm.

The fluorescent printings were carried out with a commercial inkjet printer, HP DeskJet 2132, with unbleached paper selected as the printing substrate. The blue emission ink, red emission ink, and green emission ink were filled into the backup cartridges for C, M, and Y channels, while the K channel was kept empty. All the colors of the printing patterns were finely tuned by Adobe Photoshop before printing, in order to show the best fluorescent pictures under the 254 nm UV light lamp.

Waterproof and Antiorganic Solvent Testing Method. Put the filter paper or printed nonfluorescent paper in water or the organic solvent for a period of time and then take out for drying in the air. After completely drying, place it under a UV lamp to observe and take photographs.

Fluorescence Spectrometer Measurements. Steady-state fluorescence spectra were obtained with a Hitachi F-7000 fluorescence spectrometer. Emission spectra were recorded in the range of 400−700 nm. The slit was set at 5 mm. The PMT voltage was set at a suitable voltage range from 400 to 700 V, and the scan speed was 1200 nm/min.

Fluorescence Lifetime Measurements. All the lifetime measurements are conducted under an ultrafast lifetime spectrofluorometer. The concentration of the test solutions is 25−50 μmol/L, using 280 nm excitation wavelength and 2 mm microfluorescent cell, and fluorescence attenuation curves are fitted by single exponential attenuation.

Photoluminescence Quantum Yield. All quantum yield measurements are conducted using Edinburgh instruments, FLS980 with R928PMT as the detector, a 450 W xenon lamp as the light source, and an integrating sphere accessory. The sample of micellar solution was prepared in advance with a concentration of 50 μmol/L and kept overnight before testing, and deionized water was chosen as the control.

Color Coordinate. The 1931 Commission Internationale del'Éclairage (CIE) coordinates and chromaticity diagrams were obtained from the corresponding fluorescence emission spectra using a software (CIE1931xy, model V.1.6.0.2a), according to the computational formula of the CIE standard observer.

DLS Measurements. DLS measurements were carried out using a spectrometer of standard design (ALV-5000/E/WIN multiple tau digital correlator) with a Spectra-Physics 2017 22 mW Ar laser (wavelength: 632.8 nm). The temperature was controlled at 25 ± 0.5 °C using a Haake C35 thermostat. The scattering angle was 90°, and

https://dx.doi.org/10.1021/acsami.0c10355
ACS Appl. Mater. Interfaces 2020, 12, 39578−39585

the intensity autocorrelation functions were analyzed using the method of CONTIN. Number data were recorded for all experiments.

Transmission Electron Microscopy. An FEI Tecnai G2 T20 transmission electron microscope was employed to observe the morphology of micelles. Drops of samples were put onto 230-mesh copper grids coated with the Formvar film. Excess water was removed by filter paper, and samples were then allowed to rest.

■ ASSOCIATED CONTENT

Supporting Information

The Supporting Information is available free of charge at https://pubs.acs.org/doi/10.1021/acsami.0c10355.

Supplementary experimental results for this paper (PDF)

■ AUTHOR INFORMATION

Corresponding Authors

Jianbin Huang − *Beijing National Laboratory for Molecular Sciences (BNLMS), College of Chemistry and Molecular Engineering, Peking University, Beijing 100871, China*; Email: jbhuang@pku.edu.cn

Yun Yan − *Beijing National Laboratory for Molecular Sciences (BNLMS), College of Chemistry and Molecular Engineering, Peking University, Beijing 100871, China*; orcid.org/0000-0001-8759-3918; Email: yunyan@pku.edu.cn

Authors

Tongyue Wu − *Beijing National Laboratory for Molecular Sciences (BNLMS), College of Chemistry and Molecular Engineering, Peking University, Beijing 100871, China*

Mengqi Xie − *Beijing National Laboratory for Molecular Sciences (BNLMS), College of Chemistry and Molecular Engineering, Peking University, Beijing 100871, China*

Complete contact information is available at: https://pubs.acs.org/10.1021/acsami.0c10355

Author Contributions

The manuscript was written through contributions of all authors. All authors have given approval to the final version of the manuscript.

Notes

The authors declare no competing financial interest.

■ ACKNOWLEDGMENTS

The authors are grateful to the National Natural Science Foundation of China (grant nos. 91856120, 21573011, and 21633002) and the Beijing National Laboratory for Molecular Sciences (BNLMS) for financial support.

■ REFERENCES

(1) Lin, C.; Zhuang, Y.; Li, W.; Zhou, T.-L.; Xie, R.-J. Blue, Green, and Red Full-Color Ultralong Afterglow in Nitrogen-Doped Carbon Dots. *Nanoscale* **2019**, *11*, 6584−6590.

(2) Kalytchuk, S.; Wang, Y.; Poláková, K.; Zbořil, R. Carbon Dot Fluorescence-Lifetime-Encoded Anti-Counterfeiting. *ACS Appl. Mater. Interfaces* **2018**, *10*, 29902−29908.

(3) Jia, L.; Zhang, B.; Xu, J.; Zhu, T.; Chen, R.; Zhou, F. Chameleon Luminophore for Erasable Encrypted and Decrypted Devices: From Dual-Channel, Programmable, Smart Sensory Lanthanide Hydrogel to Logic Devices. *ACS Appl. Mater. Interfaces* **2020**, *12*, 19955−19964.

(4) Ma, T.; Li, T.; Zhou, L.; Ma, X.; Yin, J.; Jiang, X. Dynamic Wrinkling Pattern Exhibiting Tunable Fluorescence for Anticounterfeiting Applications. *Nat. Commun.* **2020**, *11*, 1811.

(5) Kalita, A.; Malik, A. H.; Sarma, N. S. Stimuli-Responsive Naphthalene Diimide as Invisible Ink: A Rewritable Fluorescent Platform for Anti-Counterfeiting. *Chem.—Asian J.* **2020**, *15*, 1074−1080.

(6) Tan, H.; Gong, G.; Xie, S.; Song, Y.; Zhang, C.; Li, N.; Zhang, D.; Xu, L.; Xu, J.; Zheng, J. Upconversion Nanoparticles@Carbon Dots@Meso-SiO2 Sandwiched Core-Shell Nanohybrids with Tunable Dual-Mode Luminescence for 3D Anti-Counterfeiting Barcodes. *Langmuir* **2019**, *35*, 11503−11511.

(7) Kumar, P.; Dwivedi, J.; Gupta, B. K. Highly Luminescent Dual Mode Rare-Earth Nanorod Assisted Multi-Stage Excitable Security Ink for Anti-Counterfeiting Applications. *J. Mater. Chem. C* **2014**, *2*, 10468−10475.

(8) Yao, W.; Tian, Q.; Liu, J.; Wu, Z.; Cui, S.; Ding, J.; Dai, Z.; Wu, W. Large-Scale Synthesis and Screen Printing of Upconversion Hexagonal-Phase NaYF4:Yb^{3+},Tm^{3+}/Er^{3+}/Eu^{3+} Plates for Security Applications. *J. Mater. Chem. C* **2016**, *4*, 6327−6335.

(9) Hou, J.; Li, M.; Song, Y. Patterned Colloidal Photonic Crystals. *Angew. Chem.* **2018**, *57*, 2544−2553.

(10) Yoon, B.; Lee, J.; Park, I. S.; Jeon, S.; Lee, J.; Kim, J.-M. Recent Functional Material Based Approaches to Prevent and Detect Counterfeiting. *J. Mater. Chem. C* **2013**, *1*, 2388.

(11) Meruga, J. M.; Baride, A.; Cross, W.; Kellar, J. J.; May, P. S. Red-Green-Blue Printing Using Luminescence-Upconversion Inks. *J. Mater. Chem. C* **2014**, *2*, 2221.

(12) Reddy, C. H. V.; Siddaiah, P.; Siddaiah, P. Comparative Analysis of Dual Secure Based Medical Image Watermarking Technique to Increase Security of Watermark Data Using BFOA. *Int. J. Comp. Commun. Eng.* **2016**, *5*, 381−397.

(13) Hu, H.; Zhong, H.; Chen, C.; Chen, Q. Magnetically Responsive Photonic Watermarks on Banknotes. *J. Mater. Chem. C* **2014**, *2*, 3695.

(14) Nam, H.; Song, K.; Ha, D.; Kim, T. Inkjet Printing Based Mono-layered Photonic Crystal Patterning for Anti-counterfeiting Structural Colors. *Sci. Rep.* **2016**, *6*, 30885.

(15) Xu, J.; Zhang, B.; Jia, L.; Fan, Y.; Chen, R.; Zhu, T.; Liu, B. Dual-Mode, Color-Tunable, Lanthanide-Doped Core-Shell Nanoarchitectures for Anti-Counterfeiting Inks and Latent Fingerprint Recognition. *ACS Appl. Mater. Interfaces* **2019**, *11*, 35294−35304.

(16) Huang, W.; Xu, M.; Liu, J.; Wang, J.; Zhu, Y.; Liu, J.; Rong, H.; Zhang, J. Hydrophilic Doped Quantum Dots "Ink" and Their Inkjet-Printed Patterns for Dual Mode Anticounterfeiting by Reversible Cation Exchange Mechanism. *Adv. Funct. Mater.* **2019**, *29*, 1808762.

(17) Kanika; Kumar, P.; Singh, S.; Gupta, B. K. A Novel Approach to Synthesise a Dual-Mode Luminescent Composite Pigment for Uncloneable High-Security Codes to Combat Counterfeiting. *Chemistry* **2017**, *23*, 17144−17151.

(18) Park, M.; Kang, D.-G.; Yoon, W.-J.; Choi, Y.-J.; Koo, J.; Lim, S.-I.; Ahn, S.-k.; Jeong, K.-U. Secret Ink: Kinetically Controlled Polymorphic Superstructure of Transparent Illuminant. *Chem. Mater.* **2019**, *32*, 166−172.

(19) Nair, K. S.; Abhilash, P.; Surendran, K. P. Silica-Based Organic-Inorganic Hybrid Fluorescent Ink for Security Applications. *ACS Omega* **2019**, *4*, 2577−2583.

(20) Gangwar, A. K.; Kanika, K.; Kedawat, G.; Papanai, G. S.; Gupta, B. K. Single Excitable Dual Emissive Novel Luminescent Pigment to Generate Advanced Security Features for Anti-Counterfeiting Applications. *J. Mater. Chem. C* **2019**, *7*, 13867−13877.

(21) Trinh, C. D.; Thi Pham Hau, P.; Dung Dang, T. M.; Dang, C. M. Sonochemical Synthesis and Properties of YVO_4:Eu^{3+} Nanocrystals for Luminescent Security Ink Applications. *J. Chem.* **2019**, *2019*, 1−13.

(22) Huang, J.; Yu, Y.; Wang, L.; Wang, X.; Gu, Z.; Zhang, S. Tetraphenylethylene-Induced Cross-Linked Vesicles with Tunable Luminescence and Controllable Stability. *ACS Appl. Mater. Interfaces* **2017**, *9*, 29030−29037.

(23) Chen, D.; Cui, C.; Tong, N.; Zhou, H.; Wang, X.; Wang, R. Water-Soluble and Low-Toxic Ionic Polymer Dots as Invisible

Security Ink for MultiStage Information Encryption. *ACS Appl. Mater. Interfaces* **2019**, *11*, 1480−1486.
(24) Ma, Y.; She, P.; Zhang, K. Y.; Yang, H.; Qin, Y.; Xu, Z.; Liu, S.; Zhao, Q.; Huang, W. Dynamic Metal-Ligand Coordination for Multicolour and Water-Jet Rewritable Paper. *Nat. Commun.* **2018**, *9*, 3.
(25) Ma, Y.; Yu, Y.; She, P.; Lu, J.; Liu, S.; Huang, W.; Zhao, Q. On-Demand Regulation of Photochromic Behavior Through Various Counterions for High-Level Security Printing. *Sci. Adv.* **2020**, *6*, No. eaaz2386.
(26) Xi, G.; Sheng, L.; Du, J.; Zhang, J.; Li, M.; Wang, H.; Ma, Y.; Zhang, S. X. Water Assisted Biomimetic Synergistic Process and Its Application in Water-Jet Rewritable Paper. *Nat. Commun.* **2018**, *9*, 4819.
(27) Duan, X.; Kamin, S.; Liu, N. Dynamic Plasmonic Colour Display. *Nat. Commun.* **2017**, *8*, 14606.
(28) Sun, H.; Liu, S.; Lin, W.; Zhang, K. Y.; Lv, W.; Huang, X.; Huo, F.; Yang, H.; Jenkins, G.; Zhao, Q.; Huang, W. Smart Responsive Phosphorescent Materials for Data Recording and Security Protection. *Nat. Commun.* **2014**, *5*, 3601.
(29) Zhang, Y.; Le, X.; Jian, Y.; Lu, W.; Zhang, J.; Chen, T. 3D Fluorescent Hydrogel Origami for Multistage Data Security Protection. *Adv. Funct. Mater.* **2019**, *29*, 1905514.
(30) Sonawane, S. L.; Asha, S. K. Blue, Green, and Orange-Red Emission from Polystyrene Microbeads for Solid-State White-Light and Multicolor Emission. *J. Phys. Chem. B* **2014**, *118*, 9467−9475.
(31) Hudson, Z. M.; Lunn, D. J.; Winnik, M. A.; Manners, I. Colour-Tunable Fluorescent Multiblock Micelles. *Nat. Commun.* **2014**, *5*, 3372.
(32) Chen, L.; Hu, B.; Zhang, J.; Zhang, J.; Huang, S.; Ren, P.; Zou, Y.; Ding, F.; Liu, X.; Li, H. A Facile Synthesis of 1,3,6,8-Pyrenesulfonic Acid Tetrasodium Salt as a Hydrosoluble Fluorescent Ink for Anti-Counterfeiting Applications. *RSC Adv.* **2019**, *9*, 476−481.
(33) Sonawane, S. L.; Asha, S. K. Fluorescent Polystyrene Microbeads as Invisible Security Ink and Optical Vapor Sensor for 4-Nitrotoluene. *ACS Appl. Mater. Interfaces* **2016**, *8*, 10590−10599.
(34) Xu, Z.; Gonzalez-Abradelo, D.; Li, J.; Strassert, C. A.; Ravoo, B. J.; Guo, D.-S. Supramolecular Color-Tunable Photoluminescent Materials Based on a Chromophore Cascade as Security Inks with Dual Encryption. *Mater. Chem. Front.* **2017**, *1*, 1847−1852.
(35) Song, Z.; Lin, T.; Lin, L.; Lin, S.; Fu, F.; Wang, X.; Guo, L. Invisible Security Ink Based on Water-Soluble Graphitic Carbon Nitride Quantum Dots. *Angew. Chem.* **2016**, *55*, 2773−2777.
(36) Mahesh, S.; Lekshmi, C. L.; Renuka, K. D.; Joseph, K. Simple and Cost-Effective Synthesis of Fluorescent Graphene Quantum Dots from Honey: Application as Stable Security Ink and White-Light Emission. *Part. Part. Syst. Charact.* **2016**, *33*, 70−74.
(37) Sun, C.; Su, S.; Gao, Z.; Liu, H.; Wu, H.; Shen, X.; Bi, W. Stimuli-Responsive Inks Based on Perovskite Quantum Dots for Advanced Full-Color Information Encryption and Decryption. *ACS Appl. Mater. Interfaces* **2019**, *11*, 8210−8216.
(38) Kumar, P.; Singh, S.; Gupta, B. K. Future Prospects of Luminescent Nanomaterial Based Security Inks: From Synthesis to Anti-Counterfeiting Applications. *Nanoscale* **2016**, *8*, 14297−14340.
(39) Liu, Y.; Han, F.; Li, F.; Zhao, Y.; Chen, M.; Xu, Z.; Zheng, X.; Hu, H.; Yao, J.; Guo, T.; Lin, W.; Zheng, Y.; You, B.; Liu, P.; Li, Y.; Qian, L. Inkjet-Printed Unclonable Quantum Dot Fluorescent Anti-Counterfeiting Labels with Artificial Intelligence Authentication. *Nat. Commun.* **2019**, *10*, 2409.
(40) Andres, J.; Hersch, R. D.; Moser, J.-E.; Chauvin, A.-S. A New Anti-Counterfeiting Feature Relying on Invisible Luminescent Full Color Images Printed with Lanthanide-Based Inks. *Adv. Funct. Mater.* **2014**, *24*, 5029−5036.
(41) Zhang, C.; Yang, L.; Zhao, J.; Liu, B.; Han, M.-Y.; Zhang, Z. White-Light Emission from an Integrated Upconversion Nanostructure: Toward Multicolor Displays Modulated by Laser Power. *Angew. Chem., Int. Ed.* **2015**, *54*, 11531−11535.
(42) Zhang, D.; Zhou, W.; Liu, Q.; Xia, Z. CH3NH3PbBr3 Perovskite Nanocrystals Encapsulated in Lanthanide Metal-Organic Frameworks as a Photoluminescence Converter for Anti-Counterfeiting. *ACS Appl. Mater. Interfaces* **2018**, *10*, 27875−27884.
(43) Zhang, C.; Wang, B.; Li, W.; Huang, S.; Kong, L.; Li, Z.; Li, L. Conversion of Invisible Metal-Organic Frameworks to Luminescent Perovskite Nanocrystals for Confidential Information Encryption and Decryption. *Nat. Commun.* **2017**, *8*, 1138.
(44) Yu, X.; Wu, L.; Hu, H.; Chen, M.; Tan, Y.; Yang, D.; Pan, Q.; Zhong, Q.; Supasai, T.; Zhang, Q. Cs4PbX6 (X = Cl, Br, I) Nanocrystals: Preparation, Water-Triggered Transformation Behavior, and Anti-Counterfeiting Application. *Langmuir* **2018**, *34*, 10363−10370.
(45) Kang, H.; Lee, J. W.; Nam, Y. Inkjet-Printed Multiwavelength Thermoplasmonic Images for Anticounterfeiting Applications. *ACS Appl. Mater. Interfaces* **2018**, *10*, 6764−6771.
(46) Yao, W.; Tian, Q.; Liu, J.; Xue, Q.; Li, M.; Liu, L.; Lu, Q.; Wu, W. Preparation and RGB Upconversion Optic Properties of Transparent Anti-Counterfeiting Films. *Nanoscale* **2017**, *9*, 15982−15989.
(47) Pan, A.; Li, Y.; Wu, Y.; Yan, K.; Jurow, M. J.; Liu, Y.; He, L. Stable Luminous Nanocomposites of CsPbX3 Perovskite Nanocrystals Anchored on Silica for Multicolor Anti-Counterfeit Ink and White-LEDs. *Mater. Chem. Front.* **2019**, *3*, 414−419.
(48) Yan, Y.; de Keizer, A.; Cohen Stuart, M. A.; Besseling, N. A. M. Capacity-Controllable Nanocarriers for Metal Ions. *Soft Matter* **2009**, *5*, 790−796.
(49) Yan, Y.; Harnau, L.; Besseling, N. A. M.; de Keizer, A.; Ballauff, M.; Rosenfeldt, S.; Cohen Stuart, M. A. Spherocylindrical Coacervate Core Micelles Formed by A Supramolecular Coordination Polymer and A Diblock Copolymer. *Soft Matter* **2008**, *4*, 2207.
(50) Yan, Y.; Huang, J. Hierarchical Assemblies of Coordination Supramolecules. *Coord. Chem. Rev.* **2010**, *254*, 1072−1080.
(51) Vermonden, T.; van Steenbergen, M. J.; Besseling, N. A. M.; Marcelis, A. T. M.; Hennink, W. E.; Sudhölter, E. J. R.; Cohen Stuart, M. A. Linear Rheology of Water-Soluble Reversible Neodymium(III) Coordination Polymers. *J. Am. Chem. Soc.* **2004**, *126*, 15802−15808.
(52) Xu, L.; Jing, Y.; Feng, L.; Xian, Z.; Yan, Y.; Liu, Z.; Huang, J. The Advantage of Reversible Coordination Polymers in Producing Visible Light Sensitized Eu(III) Emissions Over EDTA via Excluding Water From the Coordination Sphere. *Phys. Chem. Chem. Phys.* **2013**, *15*, 16641−16647.
(53) Luo, J.; Xie, Z.; Lam, J. W. Y.; Cheng, L.; Tang, B. Z.; Chen, H.; Qiu, C.; Kwok, H. S.; Zhan, X.; Liu, Y.; Zhu, D. Aggregation-Induced Emission of 1-Methyl-1,2,3,4,5-Pentaphenylsilole. *Chem. Commun.* **2001**, 1740−1741.
(54) Xu, L.; Jiang, L.; Drechsler, M.; Sun, Y.; Liu, Z.; Huang, J.; Tang, B. Z.; Li, Z.; Cohen Stuart, M. A.; Yan, Y. Self-Assembly of Ultralong Polyion Nanoladders Facilitated by Ionic Recognition and Molecular Stiffness. *J. Am. Chem. Soc.* **2014**, *136*, 1942−1947.
(55) Yang, L.; Ding, Y.; Yang, Y.; Yan, Y.; Huang, J.; de Keizer, A.; Cohen Stuart, M. A. Fluorescence Enhancement by Microphase Separation-Induced Chain Extension of Eu^{3+} Coordination Polymers: Phenomenon and Analysis. *Soft Matter* **2011**, *7*, 2720.
(56) Xu, L.; Feng, L.; Han, Y.; Jing, Y.; Xian, Z.; Liu, Z.; Huang, J.; Yan, Y. Supramolecular Self-Assembly Enhanced Europium(III) Luminescence under Visible Light. *Soft Matter* **2014**, *10*, 4686−4693.
(57) Xu, L.; Xie, M.; Huang, J.; Yan, Y. Understanding the Structure of Reversible Coordination Polymers Based on Europium in Electrostatic Assemblies Using Time-Resolved Luminescence. *Langmuir* **2016**, *32*, 5830−5837.
(58) Wu, Z.; Huang, J.; Yan, Y. Electrostatic Polyion Micelles with Fluorescence and MRI Dual Functions. *Langmuir* **2015**, *31*, 7926−7933.
(59) Yan, Y.; Besseling, N. A. M.; de Keizer, A.; Marcelis, A. T. M.; Drechsler, M.; Cohen Stuart, M. A. Hierarchical Self-Assembly in Solutions Containing Metal Ions, Ligand, and Diblock Copolymer. *Angew. Chem., Int. Ed.* **2007**, *46*, 1807−1809.
(60) Yan, Y.; de Keizer, A.; Cohen Stuart, M. A.; Drechsler, M.; Besseling, N. A. M. Stability of Complex Coacervate Core Micelles

Containing Metal Coordination Polymer. *J. Phys. Chem. B* **2008**, *112*, 10908−10914.
(61) Voets, I. K.; de Keizer, A.; Cohen Stuart, M. A. Complex Coacervate Core Micelles. *Adv. Colloid Interface Sci.* **2009**, *147−148*, 300−318.
(62) Coleman, A. C.; Beierle, J. M.; Stuart, M. C. A.; Maciá, B.; Caroli, G.; Mika, J. T.; van Dijken, D. J.; Chen, J.; Browne, W. R.; Feringa, B. L. Light-Induced Disassembly of Self-Assembled Vesicle-Capped Nanotubes Observed in Real Time. *Nat. Nanotechnol.* **2011**, *6*, 547−552.
(63) Silva, J. Y. R.; da Luz, L. L.; Mauricio, F. G. M.; Vasconcelos Alves, I. B.; Ferro, J. N. d. S.; Barreto, E.; Weber, I. T.; de Azevedo, W. M.; Júnior, S. A. Lanthanide-Organic Gels as a Multifunctional Supramolecular Smart Platform. *ACS Appl. Mater. Interfaces* **2017**, *9*, 16458−16465.
(64) Mei, J.; Leung, N. L. C.; Kwok, R. T. K.; Lam, J. W. Y.; Tang, B. Z. Aggregation-Induced Emission: Together We Shine, United We Soar! *Chem. Rev.* **2015**, *115*, 11718−11940.
(65) Feng, H.-T.; Yuan, Y.-X.; Xiong, J.-B.; Zheng, Y.-S.; Tang, B. Z. Macrocycles and Cages Based on Tetraphenylethylene with Aggregation-Induced Emission Effect. *Chem. Soc. Rev.* **2018**, *47*, 7452−7476.
(66) Li, J.; Wang, J.; Li, H.; Song, N.; Wang, D.; Tang, B. Z. Supramolecular Materials Based on AIE Luminogens (AIEgens): Construction and Applications. *Chem. Soc. Rev.* **2020**, *49*, 1144−1172.
(67) Zhang, S.; Tao, Q.; Wang, Z.; Zhang, Z. Controlled Heat Release of New Thermal Storage Materials: the Case of Polyethylene Glycol Intercalated into Graphene Oxide Paper. *J. Mater. Chem.* **2012**, *22*, 20166.
(68) Mahadeva, S. K.; Kim, J. Effect of Polyethylene Oxide-Polyethylene Glycol Content and Humidity on Performance of Electro-Active Paper Actuators Based on Cellulose/Polyethylene Oxide-Polyethylene Glycol Microcomposite. *Polym. Eng. Sci.* **2010**, *50*, 1199−1204.
(69) Vermonden, T.; van der Gucht, J.; de Waard, P.; Marcelis, A. T. M.; Besseling, N. A. M.; Sudhölter, E. J. R.; Fleer, G. J.; Cohen Stuart, M. A. Water-Soluble Reversible Coordination Polymers: Chains and Rings. *Macromolecules* **2003**, *36*, 7035−7044.
(70) Biesalski, M.; Johannsmann, D.; Rühe, J. Electrolyte-Induced Collapse of A Polyelectrolyte Brush. *J. Chem. Phys.* **2004**, *120*, 8807−8814.

https://dx.doi.org/10.1021/acsami.0c10355
ACS Appl. Mater. Interfaces 2020, 12, 39578−39585